Thin Solid Films 649 (2018) 136–141

Contents lists available at ScienceDirect

Thin Solid Films

journal homepage: www.elsevier.com/locate/tsf

Preparation and characterization of copper thin film obtained by metal plasma immersion ion implantation and deposition

Demetrio Jackson dos Santos[a], Nathalie Minako Ito[a], Mara Cristina Lopes de Oliveira[a], Lara Basílio Tavares[a], Maria Cecilia Salvadori[b], Renato Altobelli Antunes[a,*]

[a] Centro de Engenharia, Modelagem e Ciências Sociais Aplicadas (CECS), Universidade Federal do ABC (UFABC), 09210-580 Santo André, SP, Brazil
[b] Instituto de Física, Universidade de São Paulo, São Paulo, SP 05389-970, Brazil

ARTICLE INFO

Keywords:
Copper
Thin films
Metal plasma ion immersion implantation and deposition
Electrochemical quartz crystal microbalance
Dissolution rate

ABSTRACT

Copper thin film was obtained by metal plasma ion immersion implantation and deposition (MePIIID). The film structure was characterized by grazing incidence X-ray diffraction whereas its thickness and surface topography were evaluated by field emission scanning electron microscopy and atomic force microscopy, respectively. Rutherford backscattering spectroscopy and X-ray photoelectron spectroscopy were used to evaluate the film chemical states. Electrochemical quartz crystal microbalance (EQCM) analysis coupled to potentiodynamic polarization was employed to investigate the dissolution behavior of the MePIIID deposited layer. The copper film presented a crystalline character and its surface chemical state was mainly comprised of Cu_2O. EQCM measurements provided good basis for estimating the thickness reduction and anodic dissolution rate of the as-deposited layer, proving to be a valuable tool for developing and evaluating copper-based MePIIID films for electronic applications.

1. Introduction

Copper and its alloys find widespread industrial applications due to their outstanding electrical and thermal conductivities [1,2]. Currently, there is a renewed interest in the corrosion behavior of these materials [3]. Such attention derives from their susceptibility to corrosion in chloride-contaminated environments which is a main issue in the electronic, pipeline and automotive industries [4–6]. Structural failure can take place due to deterioration of material's performance by chloride attack. The economic losses associated with copper corrosion are reported to be voluminous, stimulating the development of protective coatings and corrosion inhibitors [7–9]. Copper coatings can be applied in the microelectronic industry to provide a good combination of corrosion resistance and conductivity performance to electrical contacts [10,11]. However, in spite of its relative chemical stability, copper thin film corrosion is a concern in microelectronic applications.

The high sensitivity of electrochemical quartz crystal microbalance (EQCM) to mass changes has been favorably exploited to investigate deposition and dissolution of metallic thin films [12,13]. In EQCM, the mass change is obtained based on the Sauerbrey equation (Eq. (1)), where Δf is the frequency change, Δm is the mass change, f_0 é the resonant frequency, ρ_q is the quartz density, μ_q is the shear modulus of quartz and A is the electrode area exposed to the electrolyte [14].

$$\frac{\Delta f}{\Delta m} = \frac{-2\pi f_0^2}{A\sqrt{\mu_q \rho_q}} \quad (1)$$

Recently, Ralston et al. [15] employed a combination of EQCM and conventional polarization tests to study the dissolution process of magnesium in NaCl solution. EQCM proved to be reliable to monitor the online mass change either at open circuit or polarized conditions. While several authors have employed the EQCM technique to investigate the efficiency of corrosion inhibitors for copper and its alloys [16–19], the dissolution process of copper films for microelectronic applications is hardly ever reported in the literature.

Thin films obtained by the ion beam technique metal plasma immersion ion implantation and deposition (MePIIID) can have their surface chemistry easily controlled at the nanometer scale [20]. The corrosion resistance of the coated substrate can be advantageously affected by the good adhesion between the topcoat and the underlying substrate, giving rise to a robust surface treatment [21]. The use of MePIIID to produce copper films for electronic applications is hardly reported in the literature.

In this work, we investigated the dissolution process of MePIIID-deposited copper films by EQCM and potentiodynamic polarization tests. The film structure, morphology and chemical composition were studied by grazing incidence X-ray diffraction (GIXD), field emission-

* Corresponding author.
E-mail address: renato.antunes@ufabc.edu.br (R.A. Antunes).

https://doi.org/10.1016/j.tsf.2018.01.048
Received 3 September 2017; Received in revised form 23 January 2018; Accepted 23 January 2018

scanning electron microscopy (FE-SEM), atomic force microscopy (AFM), Rutherford backscattering spectroscopy (RBS) and X-ray photoelectron spectroscopy (XPS).

2. Experimental

2.1. Sample preparation

Copper films were deposited by MePIIID. The apparatus consists mainly of a plasma gun, a plasma filter and the sample holder. All components are mounted inside a stainless steel vacuum chamber. Plasma of the cathode material is obtained within the gun by a discharge between the cathode and the anode. A ceramic cylinder was applied to isolate the cathode (copper rod) from the anode. The plasma filter guides the generated copper plasma to the substrate and eliminates macroparticles. Details of the apparatus have been described in previous works [22–24]. The films were deposited using Si wafers and glassy carbon as substrates. Before deposition, the substrates were ultrasonically cleaned with acetone and isopropanol for 5 min. Next, the cleaned substrates were heated at 230 °C for 20 min. The deposition chamber pressure was approximately 7×10^{-4} Pa. High purity Cu (99.99%) was employed as cathode for obtaining the metal plasma. Plasma deposition was carried out in repetitive pulsed process. Parameters used for copper deposition were 180 A for the arc current, 5 ms of pulse duration at one pulse per second (1 Hz of frequency). The total number of pulses was 5400.

2.2. EQCM analysis

EQCM tests were carried out with AT-cut, gold-coated quartz crystals with nominal resonant frequency of 6 MHz (Autolab-Eco Chemie). Copper coating was deposited on the gold-coated quartz crystals following the same procedure described in Section 2.1. After deposition, the copper-coated crystals were rinsed in deionized water prior to EQCM analysis. After mounting the working electrodes in the EQCM cell, it was filled with 3.5 wt% NaCl solution. Electrochemical tests were conducted with a M101 Autolab potentiostat/galvanostat. Conventional three-electrode cell setup was employed with Ag/AgCl electrode as reference, a platinum wire as the auxiliary electrode and the copper-coated quartz crystals as the working electrodes. In order to ensure a steady state condition, samples were subjected to an initial monitoring of the open circuit potential. Next, potentiodynamic polarization curves were obtained at a scanning rate of $1\ mV{\cdot}s^{-1}$ in the potential range from $-250\ mV_{Ag/AgCl}$ versus the open circuit potential up to $+1.0\ V_{Ag/AgCl}$. The mass change of the working electrode was continuously recorded during the test. The tests were conducted in triplicate.

2.3. Film characterization

The atomic structure of MePIIID-deposited copper films on silicon (Si) substrates was characterized by GIXD and the crystalline phases were indexed using the JCPDS catalog. The analysis was performed using a Bruker D8 Discover theta-theta diffractometer provided with a Cu X-ray tube working at 40 kV and 40 mA, with wavelength of 0.1541 nm. A parallel beam optics configuration was used for the grazing incidence measurements with a Göbel mirror and a 0.2° divergence vertical Soller slit in the incident beam and a 0.1° divergence parallel plate horizontal slit coupled to a 0.2° vertical Soller slit in the scattered beam side. The incidence angle of the X-ray beam was fixed at 0.6° and the angular range was scanned from 10° to 60°, with a step size of 0.1° and 30 s/step.

Atomic composition of deposited cooper films was assessed by RBS. Measurements were performed using He^+ ion beam, with energy of 2.2 MeV, scattered at 120° and 170° (with respect to beam direction) and incident angle of 7°. RBS spectra were fitted using SIMNRA code.

The chemical surface state of the copper film was assessed by XPS analysis. The spectra were acquired using a ThermoFisher Scientific K-alpha$^+$ spectrometer, operating with Al-kα radiation source (1486.6 eV) at ultra-high vacuum at 10^{-9} mbar. The shift of the binding energies was calibrated with respect to C 1s hydrocarbon contamination signal at 284.8 eV. Survey spectrum and high resolution spectra for Cu2p and O1s were recorded. Background subtraction was performed using the Smart™ algorithm.

Scanning electron microscopy was performed using a FE-SEM instrument, JMS-6701-F, JEOL, in secondary electron imaging (SEI) mode operating at 10 kV to determine the thickness of the copper film deposited on the Si substrate.

Morphological characterization of the copper layer surface has been carried out by AFM using a Nanoscope IIIA, Bruker, operating in tapping mode with scanning area of $1.0 \times 1.0\ \mu m$.

3. Results and discussion

3.1. Coating characterization

GIXD analyses were carried out to assess the structure of the MePIIID-deposited copper film. As it can be observed from Fig. 1, the metallic copper arrangement was indexed as a single phase, according to the JCPDS catalog (04–0836). The peak identified as Si was indexed as the silicon phase (JCPDS 05-0565 catalog) related to the silicon wafer substrate.

Using Eq. (2) (Scherrer equation) [25,26], where $D_{(hkl)}$ is the particle size perpendicular to the diffracting lattice plane, k is a constant shape factor of 0.9, θ is the diffraction angle, λ is X-ray wavelength (0.1541 nm) and β is the full width at half maximum (FWHM), we calculated the copper average crystallite size. The peaks related to crystalline copper, (111) and (200) planes, are located at 43.43° and 50.53° (2θ), respectively. Based on their FWHM, 0.72° for (111) and 0.96° for (200), the crystallite sizes for the (111) and (200) planes were determined as 11.9 nm and 9.1 nm, respectively.

$$D_{(hkl)} = \frac{k.\lambda}{\beta.\cos\theta} \tag{2}$$

The high intensity peak observed at (111) can be associated to a face-centered cubic system of the metallic copper phase [27]. The lattice parameters were calculated according with the Bragg's Law [27] using the free software *CellCalc*. They were estimated considering a

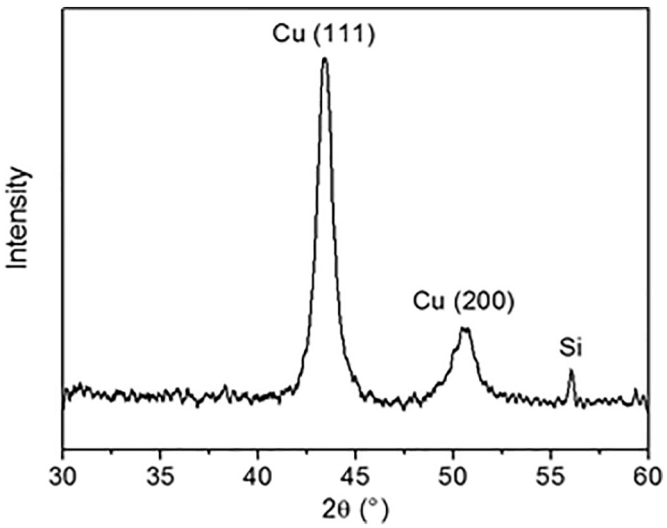

Fig. 1. GIXD pattern of the copper film obtained. The peaks were indexed as metallic copper phase according to the JCPDS catalog (04–0836). The additional peak identified as Si is related to the silicon wafer substrate (JCPDS 05-0565).

Table 1
Standard and estimated lattice parameters of the copper film.

Sample	a (Å)	V (Å^3)
JCPDS	3.615	47.24
Copper film	3.612 (± 0.005)	47.1 (± 0.2)

cubic crystallographic system. The lattice parameters of the copper structure (Table 1) showed no significant differences when compared to the JCPDS pattern, indicating that the cell is little distorted.

The copper film thickness was measured using the cross-sectional FE-SEM micrograph of the MePIIID-deposited film. Fig. 2 reveals a homogeneous copper layer with uniform thickness of some tens of nanometers (around 75 nm).

Surface morphology was investigated by AFM. Fig. 3a shows the 2D view of the as-deposited layer whereas the corresponding line scan showing the surface profile is presented in Fig. 3b. To analyze the topography of the copper surface, the average surface roughness (Ra) was determined. The difference (SD) between real surface area (SA) and projected area (PA) was also evaluated based on Eq. (3).

$$SD = \frac{SA - PA}{PA} \quad (3)$$

The mean value of Ra was 0.7 nm, while SA was 1.02 μm^2 and the calculated SD was1.7%. AFM 2D micrograph (Fig. 3a), associated with SD and Ra values, denotes the formation of a flat and smooth copper layer topography.

The nuclear scattering spectra of deposited copper are presented in Fig. 4a–b, in which the presence of O, Cu, S and Cl can be identified. The presence of S and Cl can be treated as contamination, since it is well-known that Cu oxides adsorb quickly polar contaminants [18,28,29]. Combined spectra analysis obtained under different scattering angles (170° and 120°) revealed highest O concentration at the outer metal layer (surface). The average atomic ratio Cu:O was 1.91. These results suggest the formation of copper oxides, which may be present as CuO, Cu_2O and $Cu(OH)_2$. However, RBS does not distinguish between different oxide species.

XPS analysis was, therefore, carried out to evaluate the chemical state of the MePIIID-deposited copper film. The general survey spectrum is shown in Fig. 5. The main signatures are referred to Cu2p, O1s and C1s. Since the film does not contain carbon, the C1s peak can be assigned to surface contamination (adventitious carbon) [30,31]. The concentrations of Cu2p and O1s are 44.8 at.% and 33.6 at.%, respectively. The presence of the polar contaminants S and Cl species was detected, confirming the results obtained by RBS. Auger peaks of Cu and O were also found as indicated. Narrow scan XPS spectra for the Cu2p and O1s core levels are shown in Fig. 6. The Cu2p spectrum displays a strong multiplet splitting with an energy difference of approximately 20 eV. This feature is typical of metallic copper and its oxidation states [32,33]. There are two strong peaks at 932.6 eV and 952.6 eV and a broad satellite peak at 946.7 eV. The peak at the lowest binding energy is due to $Cu2p_{3/2}$ and can be due either to Cu^0 (metallic copper) or Cu^+ species [34,35]. It is not easy to distinguish between metallic copper and Cu_2O based on the Cu2p signal, since there is a marked similarity between peak widths and binding energies of these species [36,37]. Notwithstanding, the presence of the small broad satellite peak between the two main $Cu2p_{1/2}$ and $Cu2p_{3/2}$ peaks indicates that the surface of the copper film is mainly comprised of Cu_2O [38]. Metallic copper does not present satellite peaks and CuO presents a satellite peak much more intense than that of Cu_2O [39].

Two components were assigned to the O1s core level spectrum whose peaks as indicated in Fig. 6b. The component at a binding energy of 530.5 eV can be assigned to the presence of Cu_2O [40,41]. The peak at 531.7 eV indicates that a different chemical state exists for the oxygen in the as-deposited copper film. It can be due to copper vacancy or chemisorbed O on the copper oxide [42].

SIMNRA fitting of the RBS allows estimating the thickness of the oxide layer. Assuming the formation of Cu_2O layer from XPS analysis, the thickness of the outer O rich layer thickness was 5.73 ± 0.57 nm. For the whole deposited film, an average Cu/O atomic ratio was calculated as 6.72. In spite of the decreased O content across the MePIIID film with respect to the oxygen-rich outer layer, the presence of O suggests the existence of copper oxide species in lower contents through the film thickness.

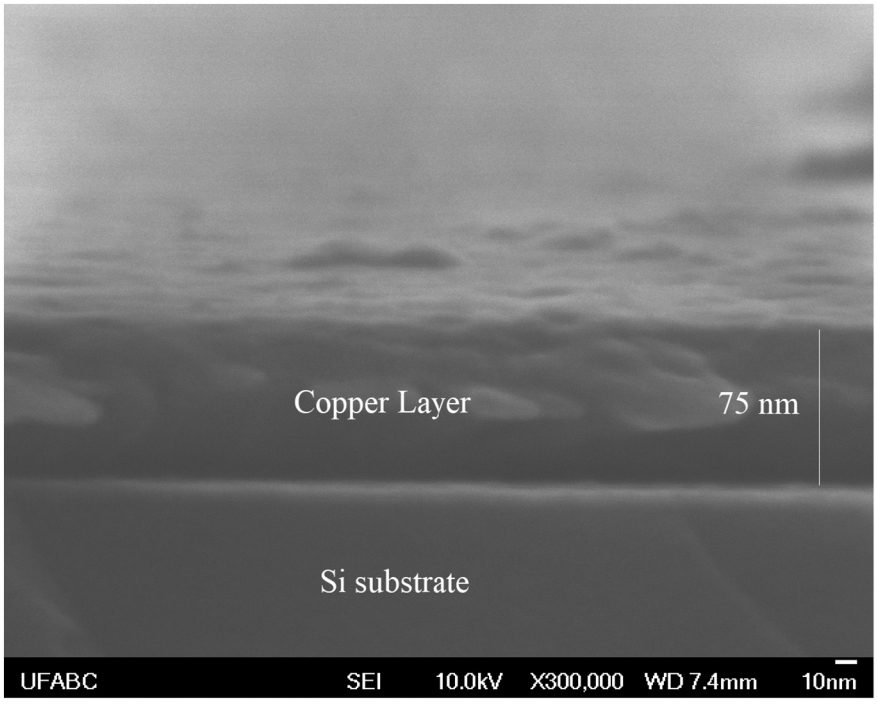

Fig. 2. FE-SEM micrograph of the cross section of the MePIIID copper film (tilt angle 10°).

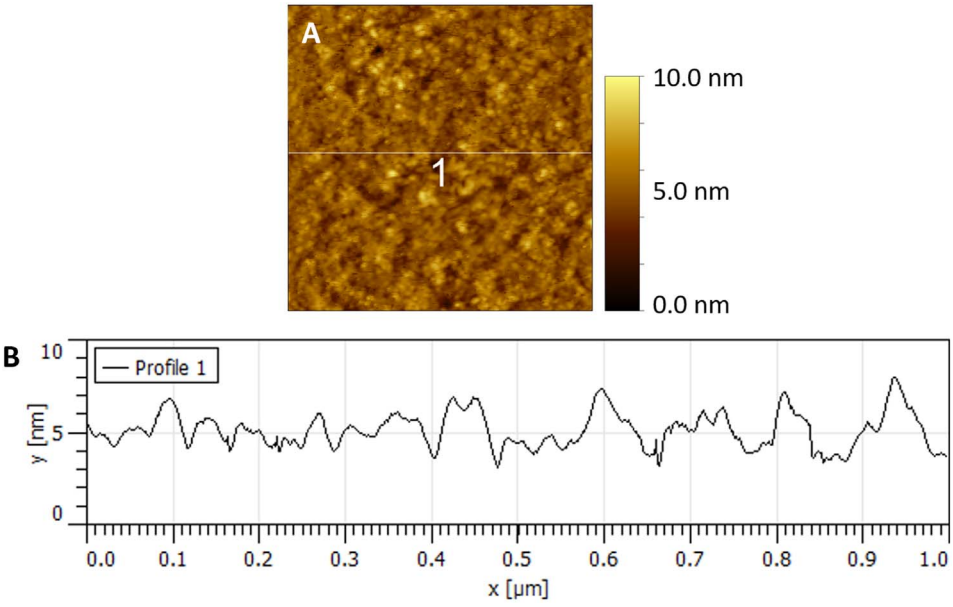

Fig. 3. AFM topographic images of the MePIIID copper film: A. 2-D (scan size: 1.0 µm × 1.0 µm; *Z*-range: 10.0 nm); B. Cross section roughness profile extract from line "1" represented in A.

3.2. EQCM measurement

Fig. 7a shows the mass change (Δm) recorded with the EQCM on the copper film when it was polarized in 3.5 wt% NaCl solution at room temperature. It is possible to estimate the film thickness reduction rate (δ) from the mass change results using Eq. (4) [17] where A is the electrode surface area exposed to the electrolyte, ρ is the copper density and t is the time. The result is shown in Fig. 7b. The corresponding potentiodynamic polarization curve is shown in Fig. 7c.

$$\delta = \frac{\Delta m}{A.\ \rho.\ t} \tag{4}$$

The mass change was negligible until the potential reaches approximately $-0.17\ V_{Ag/AgCl}$. At this stage there is an initial mass loss up to $-0.04\ V_{Ag/AgCl}$, followed by a small plateau denoting a new period of null mass loss that takes places up to $0.09\ V_{Ag/AgCl}$. Then, a new plateau of null mass loss ensues from 0.23 up to $0.80\ V_{Ag/AgCl}$. This plateau is followed by a very sharp mass loss up to end of the test. The thickness reduction rate presents an obvious coincidence with the EQCM mass change. It is interesting to note that the thickness reduction at the end of the test was approximately 72 nm. This value is in good agreement with the copper film thickness determined from the FE-SEM micrograph presented in Fig. 2. The copper film was, therefore, completely consumed during the EQCM measurement, exposing the gold-coated quartz crystal substrate.

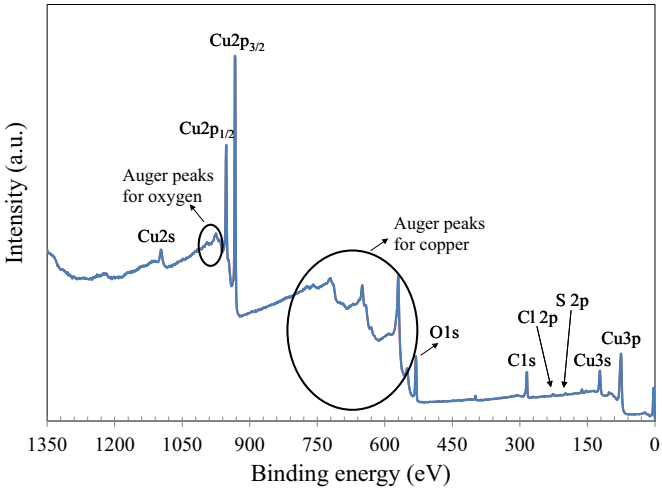

Fig. 5. XPS survey spectrum for the as-deposited copper film.

The mass loss behavior can be correlated with the corresponding potentiodynamic polarization curve (Fig. 7c). The corrosion potential (E_{corr}) is $-0.48\ V_{Ag/AgCl}$. The curve presents a typical passive region which spans from -0.05 up to $0.78\ V_{Ag/AgCl}$. The passive current density (i_{pass}) was defined at the middle of the passive range [43] and is

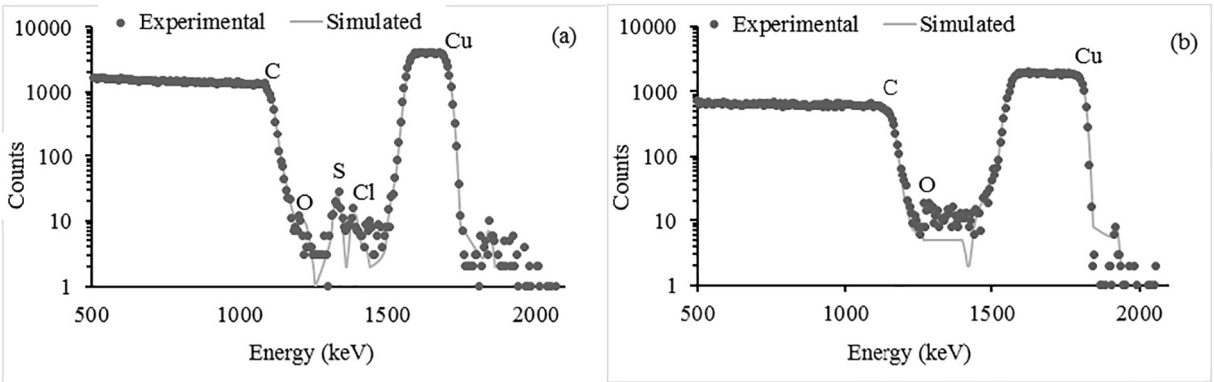

Fig. 4. Nuclear scattering spectra for the deposited copper film for following scattering and incident angles: (a) energy spectra of 2.2-MeV He^+ ions scattered to 170° (7°incidence angle); (b) energy spectra of 2.2-MeV He^+ ions scattered to 120° (7° incidence angle).

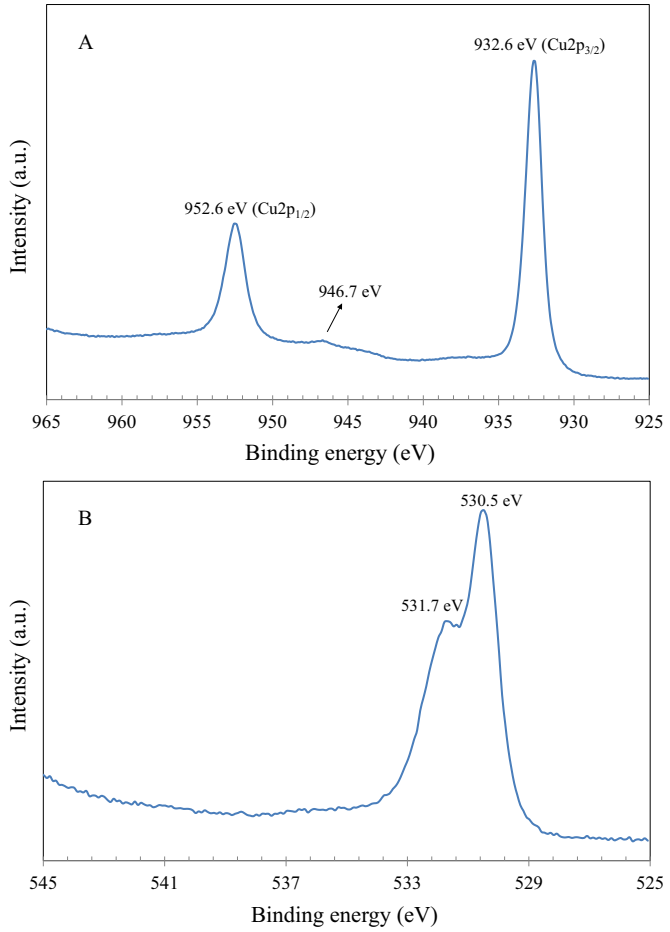

Fig. 6. Narrow scan XPS spectra of the as deposited copper film: a) Cu2p and b) O1s core levels.

equal to $1.58.10^{-4}$ A·cm^{-2}. The first period of negligible mass change encompasses the cathodic region of the polarization curve, extending up to -0.17 $V_{Ag/AgCl}$ which is located above the corrosion potential of the copper film and corresponds to the end of the anodic dissolution step that occurs before the electrode surface reaches the passive state. The wide plateau of null mass change between 0.23 up to 0.80 $V_{Ag/AgCl}$ corresponds to the point at which the copper film is in the passive region. At the end of the passive region there is a typical steep increase of the current density due to passive film breakdown in the presence of chloride ions [44]. The pitting potential (E_{pit}) was 0.77 $V_{Ag/AgCl}$. This corresponds to the sudden and sharp drop of the mass change up to the end of the test. After this point, the current density decreases near the end of the test which can be due to the fact that the copper film was completely consumed, exposing the gold-coated quartz crystal, as discussed above. The current density decreased due to the high corrosion resistance of the gold surface.

The EQCM current density (i_{corr}) could be estimated using the Faraday's law, according to Eq. (5) [45] where F is the Faraday's constant, M_{Cu} is the copper atomic mass (63.54 g/mol) and z (the copper ion charge) was taken as +1, based on the XPS results that pointed to the oxidation of the copper film to the Cu_2O state.

$$i_{corr} = \left(\frac{dm}{dt}\right).\frac{z.F}{M_{Cu}} \quad (5)$$

The mass loss rate (dm/dt) was determined from Fig. 7a by considering the potential interval between the beginning of the first detectable mass change and the end of the test (which corresponds to the whole interval wherein the mass loss was detected). The value of i_{corr} determined from the EQCM measurement is approximately

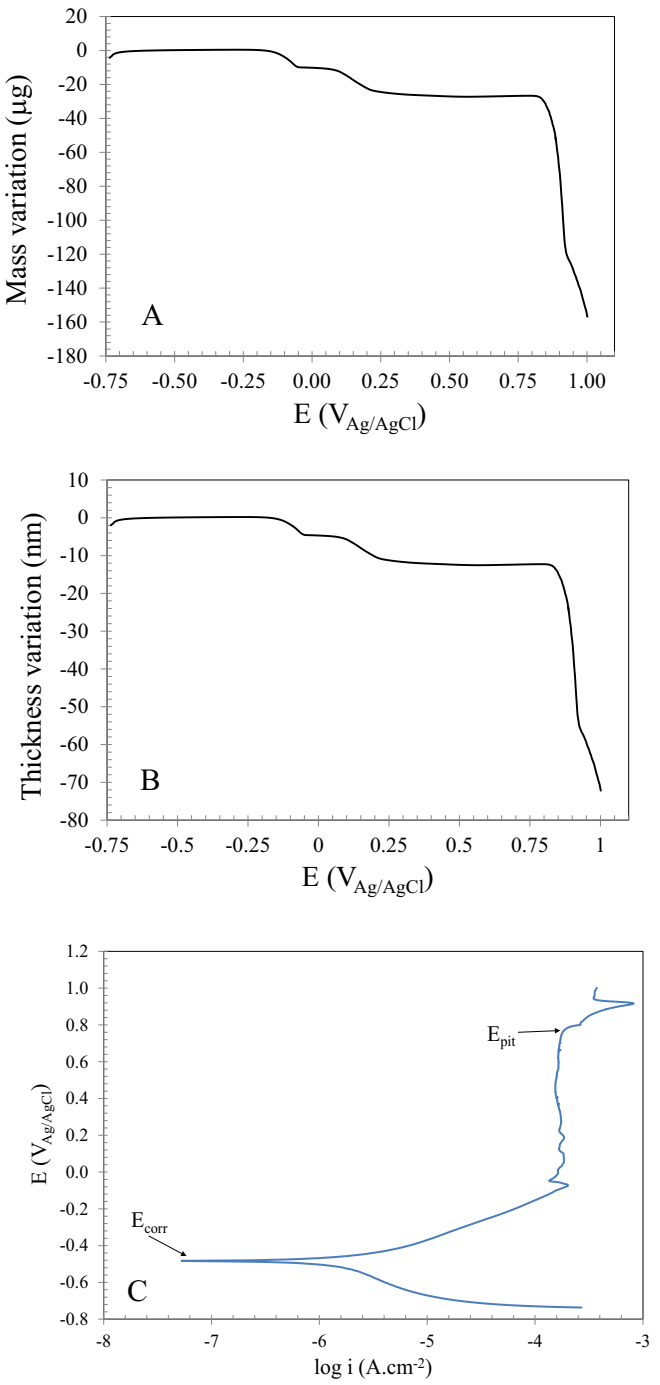

Fig. 7. a) Mass change recorded with the EQCM on the copper film when polarized in 3.5 wt% NaCl solution at room temperature; b) Thickness reduction rate; c) corresponding potentiodynamic polarization curve.

$2.05.10^{-4}$ A·cm^{-2} which is in good agreement with the value of i_{pass} determined from the potentiodynamic polarization curve. Since the potentiodynamic polarization curve of the copper film indicated a typical passive behavior, anodic dissolution is controlled by i_{pass} [46]. In this respect, i_{corr} determined by EQCM and i_{pass} determined from the passive region of the polarization curve gave good approximation for the copper film dissolution rate. The results suggest that EQCM can be employed to provide a reliable evaluation of the dissolution process of copper films deposited by MePIIID for electronic applications.

4. Conclusions

A thin, crystalline copper film was successfully obtained by MePIIID. Its surface chemical state was mainly comprised of Cu_2O. Oxygen is present in the Cu_2O layer and is likely also present as a chemisorbed species. EQCM analysis indicated that the dissolution rate of the copper film is $2.05 \cdot 10^{-4}$ A·cm^{-2}. This result is in good agreement with the anodic dissolution rate determined from potentiodynamic polarization test. The thickness of the copper was estimated as 72 nm from the EQCM analysis which agrees well with the thickness determined from cross-sectional FE-SEM analysis. EQCM proved to be a valuable tool for evaluating the dissolution rate of copper films produced by MePIIID.

Acknowledgments

The authors are thankful to Brazilian agency FINEP for the financial support to the present work (Proc. 04.13.0096.01).

References

[1] M. Mousavi, T. Baghgoli, Application of interaction energy in quantitative structure-inhibition relationship study of some benzenethiol derivatives on copper, Corros. Sci. 105 (2016) 170–175.
[2] T.T. Qin, J. Li, H.Q. Luo, M. Li, N.B. Li, Corrosion inhibition of copper by 2,5-dimercapto-1,3,4-thiadiazole monolayer in acidic solution, Corros. Sci. 53 (2011) 1072–1078.
[3] H. Yu, C. Li, B. Yuan, C. Wang, The inhibitive effects of AC-treated mixed self-assembled on copper corrosion, Corros. Sci. 120 (2017) 231–238.
[4] Y. Qiang, S. Zhang, S. Xu, W. Li, Experimental and theoretical studies on the corrosion inhibition of copper by two indazole derivatives in 3.0% NaCl solution, J. Colloid Interface Sci. 472 (2016) 52–59.
[5] W. Chen, S. Hong, H.B. Li, H.Q. Luo, M. Li, N.B. Li, Protection of copper corrosion in 0.5 M NaCl solution by modification of 5-mercapto-3-phenyl-1,3,4-thiadiazole-2-thione potassium self-assembled monolayer, Corros. Sci. 61 (2012) 53–62.
[6] Y. Yu, Y. Wang, J. Li, D. Zhang, L. Gao, In situ click-assembling monolayers on copper surface with enhanced corrosion resistance, Corros. Sci. 113 (2016) 133–144.
[7] S. Hong, W. Chen, Y. Zhang, H.Q. Luo, M. Li, N.B. Li, Investigation of the inhibition effect of trithiocyanuric acid on corrosion of copper in 3.0 wt% NaCl, Corros. Sci. 66 (2013) 308–314.
[8] S. Hsieh, W.J. Chao, P.Y. Lin, C.W. Hsieh, Influence of molecular packing on the corrosion inhibition properties of self-assembled octadecyltrichlorosilane monolayers on silicon, Corros. Sci. 80 (2014) 427–433.
[9] M.B.P. Mihajlovic, M.B. Radovanovic, Z.Z. Tasic, M.M. Antonijevic, Imidazole based compounds as copper corrosion inhibitors in seawater, J. Mol. Liq. 225 (2017) 127–136.
[10] M. Winnicki, A. Malachowska, A. Baszczuk, M. Rutkowska-Gorczyca, D. Kukla, M. Lachowicz, A. Ambroziak, Surf. Coat. Technol. 318 (2017) 90–98.
[11] N.G. Mistkawi, M.A. Hussein, M. Ziomek-Moroz, S.B. Rananavare, Corrosion behavior of copper thin films in organic HF-containing cleaning solution for semiconductor applications, J. Electrochem. Soc. 157 (2010) C24–C29.
[12] A. Collazo, R. Figueroa, X.R. Nóvoa, C. Pérez, Corrosion of electrodeposited Sn in 0.01 M NaCl solution. A EQCM and EIS study, Electrochim. Acta 202 (2016) 288–298.
[13] M. Hattori, Y. Oda, EQCM analysis of titanium corrosion in peroxide- or fluoride-containing solutions, Bull. Tokyo Dent. Coll. 54 (2013) 135–140.
[14] D.A. Buttry, M.D. Ward, Measurement of interfacial processes at electrode surfaces with the electrochemical quartz crystal microbalance, Chem. Rev. 92 (1992) 1355–1379.
[15] K.D. Ralston, S. Thomas, G. Williams, N. Birbilis, An electrochemical quartz crystal microbalance study of magnesium dissolution, Appl. Surf. Sci. 360 ((2016) 342–348.
[16] M. Fonsati, F. Zucchi, G. Trabanelli, Study of corrosion inhibition of copper in 0.1 M NaCl using the EQCM technique, Electrochim. Acta 44 (1998) 311–322.
[17] J. Telegdi, A. Shaban, E. Kálmán, EQCM study of copper and iron corrosion inhibition in presence of organic inhibitors and biocides, Electrochim. Acta 45 (2000) 3639–3647.
[18] M. Finsgar, EQCM and XPS analysis of 1,2,4-triazole and 3-amino-1,2,4-triazole as copper corrosion inhibitors in chloride solution, Corros. Sci. 77 (2013) 350–359.
[19] H. Tian, Y.F. Cheng, W. Li, B. Hou, Triazolyl-acylhydrazone derivatives as novel inhibitors for copper corrosion in chloride solutions, Corros. Sci. 100 (2015) 341–352.
[20] A. Anders, Metal plasma immersion ion implantation and deposition: a review, Surf. Coat. Technol. 93 (1997) 158–167.
[21] B.-S. Kang, T.-T. Sul, Y. Jeong, E. Byon, J.-K. Kim, S. Cho, S.-J. Oh, T. Albrektsson, Metal plasma immersion ion implantation and deposition (MePIIID) on screw-shaped titanium implant: the effects of ion source, ion dose and acceleration voltage on surface chemistry and morphology, Med. Eng. Phys. 33 (2011) 730–738.
[22] J. Ferreira, F.S. Teixeira, A.R. Zanatta, M.C. Salvadori, R. Gordon, O.N. Oliveira Jr., Tailored SERS substrates obtained with cathodic arc plasma ion implantation of gold nanoparticles into a polymer matrix, Phys. Chem. Chem. Phys. 14 (2012) 2050–2055.
[23] M.C. Salvadori, I.G. Brown, A.R. Vaz, L.L. Melo, M. Cattani, Measurement of the elastic modulus of nanostructured gold and platinum thin films, Phys. Rev. B 67 (2003) 153404-1–153404-4.
[24] F.S. Teixeira, W.W.R. Araújo, N.K. Gushiken, M. Cattani, M.C. Salvadori, On the influence of PDMS (polydimethylsiloxane) substrate surface energy in wrinkling of DLC (diamond-like carbon) thin films, J. Appl. Phys. 122 (2017) 135308-1–135308-6.
[25] R.B. Heimann, H.D. Lehmann, Bioceramic Coatings for Medical Implants: Trends and Techniques, John Wiley & Sons, 2015.
[26] T. Theivasanthi, M. Alagar, X-ray diffraction studies of copper nanopowder, Arch. Res. Phys. 1 (2010) 112–117.
[27] B.D. Cullity, Elements of X-ray Diffraction, Addison-Wesley Publishing Company, Inc., 1956.
[28] M. Finšgar, 2-Mercaptobenzimidazole as a copper corrosion inhibitor: part II. Surface analysis using X-ray photoelectron spectroscopy, Corros. Sci. 72 (2013) 90–98.
[29] P.E. Laibinis, G.M. Whitesides, D.L. Allara, Y.T. Tao, A.N. Parikh, R.G. Nuzzo, Comparison of the structures and wetting properties of self-assembled monolayers of n-alkanethiols on the coinage metal surfaces, copper, silver, and gold, J. Am. Chem. Soc. 113 (1991) 7152–7167.
[30] F. Cocco, B. Elsener, M. Fantauzzi, D. Atzei, A. Rossi, Nanosized surface films on brass alloys by XPS and XAES, RCS Adv. 6 (2016) 31277–31289.
[31] J. Deuermeier, J. Gassmann, J. Brötz, A. Klein, Reactive magnetron sputtering of Cu_2O: dependence on oxygen pressure and interface formation with indium tin oxide, J. Appl. Phys. 109 (2011) 113704-1–113704-7.
[32] C. Zhu, A. Osherov, M.J. Panzer, Surface chemistry of electrodeposited Cu_2O films studied by XPS, Electrochim. Acta 111 (2013) 771–778.
[33] X. Yu, Y. Wei, L. Huang, J. Niu, J. Zhang, X. Li, B. Yao, Fabrication, morphology formation mechanism and properties of nanometer Cu_2O thin film with KCl-doping, Mater. Chem. Phys. 148 (2014) 727–733.
[34] Y. Wan, Y. Zhang, X. Wang, Q. Wang, Electrochemical formation and reduction of copper oxide nanostructures in alkaline media, Electrochem. Commun. 36 (2013) 99–102.
[35] K. Mansikkamäki, U. Haapanen, C. Johans, K. Kontturi, M. Valden, Adsorption of benzotriazole on the surface of copper alloys studied by SECM and XPS, J. Electrochem. Soc. 153 (2006) B311–B318.
[36] J. Hernandez, P. Wrschka, G.S. Oehrlein, Surface chemistry studies of copper chemical mechanical planarization, J. Electrochem. Soc. 148 (2001) G389–G397.
[37] S.D. Giri, A. Sarkar, Electrochemical study of bulk and monolayer copper in alkaline solution, J. Electrochem. Soc. 163 (2016) H252–H259.
[38] M. Watanabe, H. Ando, T. Handa, T. Ichino, N. Kuwaki, Comparative XPS study of silver and copper surfaces exposed to flowing air containing low concentration of sulfur dioxide, Zairyo-to-Kankyo 56 (2007) 10–15.
[39] G. Schön, ESCA studies of Cu, Cu_2O and CuO, Surf. Sci. 35 (1973) 96–108.
[40] S. Poulston, P.M. Parlett, P. Stone, M. Bowker, Surface oxidation and reduction of CuO and Cu_2O studied using XPS and XAES, Surf. Interface Anal. 24 (1996) 811–820.
[41] H. Chen, J.-H. Lee, Y.-H. Kim, D.-W. Shin, S.-C. Park, X. Meng, J.-B. Yoo, Metallic copper nanostructures synthesized by a facile hydrothermal method, J. Nanosci. Nanotechnol. 10 (2010) 629–636.
[42] S. Dolai, S. Das, S. Hussain, R. Bhar, A.K. Pal, Cuprous oxide (Cu_2O) thin films prepared by reactive d.c. sputtering, Vacuum 141 (2017) 296–306.
[43] S. Ningshen, M. Sakairi, K. Suzuki, S. Ukai, The corrosion resistance and passive film compositions of 12% Cr and 15% Cr oxide dispersion strengthened steels in nitric acid media, Corros. Sci. 78 (2014) 322–334.
[44] D. Starosvetsky, O. Khaselev, M. Auinat, Y. Ein-Eli, Initiation of copper dissolution in sodium chloride electrolytes, Electrochim. Acta 51 (2006) 5660–5668.
[45] K. Rahmouni, N. Hajjaji, M. Keddam, A. Srhiri, H. Takenouti, The inhibiting effect of 3-methyl 1,2,4-triazole 5-thione on corrosion of copper in 3% NaCl in presence of sulphide, Electrochim. Acta 52 (2007) 7519–7528.
[46] S. Hiromoto, E. Onodera, A. Chiba, K. Asami, T. Hanawa, Microstructure and corrosion behaviour in biological environments of the new forged low-Ni Co-Cr-Mo alloys, Biomaterials 26 (2005) 4912–4923.